Pis'ma v ZhETF, vol. 83, iss. 8, pp. 399 – 404 April 25

Spin-orbit lateral superlattices: energy bands and spin polarization in 2DEG

V. Ya. Demikhovskii, D. V. Khomitsky[1)]

Department of Physics, University of Nizhny Novgorod, 603950 Nizhny Novgorod, Russia

Submitted 14 March 2006

The Bloch spinors, energy spectrum and spin density in energy bands are studied for the two-dimensional electron gas (2DEG) with Rashba spin-orbit (SO) interaction subject to one-dimensional (1D) periodic electrostatic potential of a lateral superlattice. The space symmetry of the Bloch spinors with spin parity is studied. It is shown that the Bloch spinors at fixed quasimomentum describe the standing spin waves with the wavelength equal to the superlattice period. The spin projections in these states have the components both parallel and transverse to the 2DEG plane. The anticrossing of the energy dispersion curves due to the interplay between the SO and periodic terms is observed, leading to the spin flip. The relation between the spin parity and the interband optical selection rules is discussed, and the effect of magnetization of the SO superlattice in the presence of external electric field is predicted.

PACS: 73.21.Cd, 85.75.-d

Introduction. In the past years, an increasing attention has been drawn to the spin related phenomena in semiconductor structures. This research area has developed in the new branch of condensed matter physics and spin electronics. The problem of spin-dependent quantum states and transport phenomena in these systems are currently attracting a lot of interest also due to their potential for future electronic device applications.

In two-dimensional semiconductor heterostructures the spin-orbit (SO) interaction is usually dominated by the Rashba coupling [1] stemming from the structure inversion asymmetry of confining potential. The low-dimensional semiconductor structures with SO interaction were studied theoretically in numerous papers [2 – 5], including the 1D periodic systems with SO coupling [6 – 8].

The effects of spin splitting in two-dimensional electron gas (2DEG) were investigated experimentally by the magnetotransport studies, in particular, by Shubnikov – de Haas oscillations [9]. The role of other SO terms, such as Dresselhaus term, can be estimated, for example, by optical methods [10]. As it was demonstrated by the experiments, in the SO structures interesting effects may be observed, such as the spin Hall effect [11] and the spin-galvanic effect [12].

In the present paper we study quantum states and the electron spin distribution in a system combining the spin-splitting phenomena caused by the SO interaction and the external gate-controlled periodic electric potential. We thus want to investigate the spin orientation and spin polarization that can be achieved in currently manufactured gated semiconductor structures with lateral surface superlattice. For example, the 1D superlattice can be fabricated by the metal gate evaporation with typical period of 50–200 nm. We use the value of lateral period in the x-direction to be $a = 60$ nm which gives us the energy scale $\pi^2\hbar^2/2ma^2$ of the order of 2 meV for the effective mass $m^* = 0.067m_0$ in GaAs. The values of Rashba coupling constant for the most important semiconductors are in the range of $(1 \dots 5) \cdot 10^{-11}$ eV·m. It is known also that the Rashba coupling strength can be modified by the gate field by up to 50% [13]. Below in our calculations we use the value $\alpha = 5 \cdot 10^{-11}$ eV·m which gives the typical shift of the parabolic dispersion curves k_{SO} to be of the order of π/a. So, in the structure studied in the manuscript the electron kinetic energy $\pi^2\hbar^2k^2/2m$ will be comparable to the Rashba energy αk which makes the effects of SO interaction and periodic potential distinguishable. It should be mentioned also that the energy scale studied in our paper means that the effects discussed in the manuscript can be clearly observed experimentally at helium temperatures.

1. Quantum states. The Hamiltonian of our problem

$$\hat{H} = \hat{H}_0 + V(x) \tag{1}$$

is the sum of the Rashba Hamiltonian $\hat{H}_0$ with the SO coupling strength α,

$$\hat{H}_0 = \frac{\hat{p}^2}{2m^*} + \alpha(\hat{\sigma}_x\hat{p}_y - \hat{\sigma}_y\hat{p}_x), \tag{2}$$

[1)] e-mail: khomitsky@phys.unn.ru

and the 1D periodic potential $V(x)$ of a 1D superlattice with the period a. We choose the simplest form of the periodic potential

$$V(x) = V_0 \cos \frac{2\pi x}{a}, \tag{3}$$

where the sign and the magnitude of V_0 can be controlled, for example, by an external gate, leaving us a wide interval of possible V_0 amplitudes with an order of several meV.

1.1. Perturbation approach. Qualitatively the formation of the SO-split bands can be seen in the perturbation approach applied in the problem of quantum states in quantum wires [4] and in the tight-binding approximation for the SO superlattices [8]. Namely, at $k_y = 0$ the Hamiltonian (1) is written as $\hat{p}^2/2m^* + V(x) - \alpha\hat{\sigma}_y\hat{p}_x$. Considering the SO terms $-\alpha\hat{\sigma}_y\hat{p}_x$ as a perturbation, one can choose the zero-order wavefunction as

$$\Psi(x) = \psi_{mk}(x) \begin{pmatrix} 1 \\ \pm i \end{pmatrix}, \tag{4}$$

where $\psi_{mk}(x)$ are the eigenstates of the Hamiltonian $\hat{p}^2/2m^* + V(x)$ and m is the band number. Thus, in the first order of the perturbation theory the energy spectrum will be determined by the expression

$$E_m(k_x, k_y = 0) = \varepsilon_m(k_x) \pm \frac{\hbar k_{\mathrm{SO}}}{m^*} \frac{\partial \varepsilon_m}{\partial p_x}, \tag{5}$$

where $\varepsilon_m(k_x)$ is the band spectrum in the 1D periodic potential $V(x)$ without the SO interaction. Here we have used the relation $(1/m^*)\langle\psi_{mk} \mid \hat{p}_x \mid \psi_{mk}\rangle = \partial\varepsilon_m/\partial p_x$ for derivation of Eq.5. An example of the energy band spectrum of two lowest bands at $k_y = 0$ each double-split by the SO interaction is given in Fig.1. One can see that since the derivative $\partial\varepsilon_m/\partial p_x$ vanishes at the border of the Brillouin zone (BZ) $k_x = \pm\pi/a$, $k_y = 0$ and at the BZ center, the degeneracy is not lifted in these points, being lifted at finite k_y only.

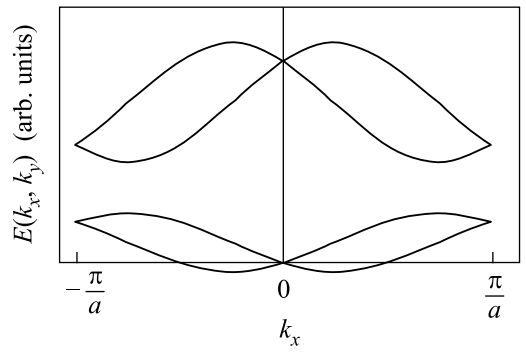

Fig.1. Energy bands at $k_y = 0$ double-split by the SO perturbation. The degeneracy is not lifted at $k_x = 0, \pm\pi/a$, $k_y = 0$ since the derivative $\partial\varepsilon_m/\partial p_x$ of the unperturbed band dispersion vanishes at these points

1.2. Bloch spinors. In the presence of both SO coupling and periodic potential we construct the two-component eigenstate of the Hamiltonian (1)

$$\psi_{\mathbf{k}}(x, y) = e^{ik_y y} \begin{pmatrix} \psi^1_{\mathbf{k}}(x) \\ \psi^2_{\mathbf{k}}(x) \end{pmatrix} \tag{6}$$

as a superposition of two-component spinors which are the eigenstates of the Rashba Hamiltonian (2). The wavevectors of the basis states in this superposition are shifted by the reciprocal lattice vector $\mathbf{b}$ of the supelattice:

$$\mathbf{k}_n = \mathbf{k} + n\mathbf{b} = \left(k_x + \frac{2\pi}{a}n, \quad k_y\right), \tag{7}$$

$n = 0, \pm1, \pm2, \ldots$ The eigenstate in band m thus has the form

$$\psi_{m\mathbf{k}} = \sum_{\lambda n} a^m_{\lambda n}(\mathbf{k}) \frac{e^{i\mathbf{k}_n \mathbf{r}}}{\sqrt{2}} \begin{pmatrix} 1 \\ \lambda e^{i\theta_n} \end{pmatrix}, \quad \lambda = \pm1, \tag{8}$$

where $\mathbf{k}$ is the quasimomentum in the 1D BZ and $\theta_n = \arg[k_y - ik_{nx}]$. After substituting the wavefunction (8) into the Schrödinger equation the coefficients $a^m_{\lambda n}$ are determined by the standard eigenvalue problem

$$\sum_{\lambda' n'} \left[\left(E^R_{n'\lambda'} - E\right) \delta_{\lambda n \lambda' n'} + V^{\lambda\lambda'}_{nn'} \right] a^m_{\lambda' n'} = 0, \tag{9}$$

where $E^R_{\lambda n}$ is the energy of a free Rashba quantum state

$$E^R_\lambda = \hbar^2 k^2/2m + \lambda\alpha k \tag{10}$$

taken at the point in $\mathbf{k}$-space defined by (7), i.e. $E^R_{n\lambda} = E^R_\lambda(k_x + 2\pi n/a, k_y)$. The matrix elements in the system (9) have the form

$$\begin{gathered} V^{\lambda\lambda'}_{nn'} = V_0 A_{nn'}(1 + \lambda\lambda' e^{i(\theta_n - \theta_{n'})}), \\ A_{nn'} = \tfrac{1}{2}\delta_{n,n'\pm1}, \quad n = n' \pm 1. \end{gathered} \tag{11}$$

The structure of matrix elements (11) determines the classification of energy bands and gaps in the SO superlattice. The dependence of the matrix elements (11) on the quantum numbers k_x and k_y can be obtained directly from Eq.(11). The matrix elements $V^{+-}_{n,n\pm1}$ and $V^{-+}_{n,n\pm1}$ describe the coupling between the nearest-neighboring states (7) with $n' = n \pm 1$ and with the opposite indices $\lambda \neq \lambda'$ labeling different up- and down-Rashba bands (10). Here the superscript $\pm$ labels the index $\lambda = \pm1$.

We shall see below that these elements produce the energy gaps located inside the BZ. The elements $V^{++}_{n,n\pm1}$ and $V^{--}_{n,n\pm1}$ are responsible for the coupling between the states of the same Rashba index $\lambda = \lambda'$. Such elements could open gaps on the borders of the BZ $k_x = \pm\pi/a$. However, one can see from (11) that they vanish for the case of pure electrostatic periodic potential. Then, for the values of at $k_y \gg \pi/a$ the elements with opposite indices $\lambda \neq \lambda'$, i.e. $V^{+-}_{n,n\pm1}$ and $V^{-+}_{n,n\pm1}$ decrease to zero while the elements with $\lambda = \lambda'$ approach their maximum values.

1.3. Energy spectrum. The energy spectrum calculated with the help of system (9) is shown in Fig.2. Here

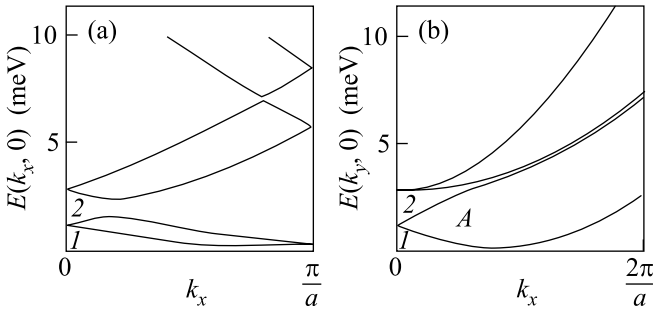

Fig.2. Energy spectrum at $\alpha = 5 \cdot 10^{-11}$ eV·m, $V_0 = 1.7$ meV shown (a) as a function of k_x at $k_y = 0$ and (b) as a function of k_y at $k_x = 0$. In the latter case the anticrossing takes place at the point A for band 2

in Fig.2a we give an example of energy spectrum $E(k_x)$ at fixed $k_y = 0$ and in Fig.2b the k_y-dependence of the same spectrum for $k_x = 0$. In accordance with the Kramers theorem the symmetry $E_{m\uparrow}(\mathbf{k}) = \mathbf{E}_{\mathbf{m}\downarrow}(-\mathbf{k})$ together with the symmetry $k_{x,y} \to -k_{x,y}$ takes place, and we thus show the spectrum only at positive k_x and k_y. One can see that the spin degeneracy at $k_y = 0$ is not lifted at the center and at the borders of the BZ $k_x = \pm\pi/a$. This result was also obtained earlier in the perturbation approach, see Fig.1. The nature of this effect is due to the specific k_x and k_y dependence of matrix elements (11). The elements $V^{\lambda=\lambda'}_{nn\pm1}$ which are responsible for the degeneracy lifting at $k_x = \pm\pi/a$ and $k_y = 0$ vanish at $k_y = 0$. The other set of elements $V^{\lambda=-\lambda'}_{nn\pm1}$ is non-zero at $k_y = 0$, and it opens the gaps inside the BZ. The k_y-dependence of the energy bands at $k_x = 0$ is shown in Fig.2b. The degeneracy at $k_y = 0$ is lifted at finite k_y by mutual influence of linear k_y terms in (2) and by the matrix elements (11). At certain conditions the anticrossing of the dispersion curves from different bands [4] may take place. An example of the anticrossing effect can be see in Fig.2b near the point A for the band 2. Below we shall see that the anticrossing leads to the spin flip in the (k_x, k_y) plane for quantum states near the anticrossing point.

2. Spin polarization. The control on the spin polarization is crucial for practical implementation of spintronics. Below we show that in the SO superlattice the standing spin wave with the period equal to the superlattice period is formed. We discuss the space distribution of the spin density for the states with different quasimomenta $\mathbf{k}$ and the distribution of spin expectation values in the BZ. The latter describes the mean value of spin polarization for the electrons travelling in different directions. We have calculated the spin density

$$S_{i\mathbf{k}}(x, y) = (\psi_{\mathbf{k}})^{\dagger}\hat{\sigma}_i\psi_{\mathbf{k}} \tag{12}$$

for a quantum state $\psi_{\mathbf{k}}$ in a given band and after the space integration we obtained the vector field of 2D spin expectation values $(\sigma_x(\mathbf{k}), \sigma_y(\mathbf{k}))$ in the BZ:

$$\sigma_i(\mathbf{k}) = \langle\psi_{\mathbf{k}} \mid \hat{\sigma}_i \mid \psi_{\mathbf{k}}\rangle. \tag{13}$$

In Fig.3 we show the calculated distribution of (σ_x, σ_y)

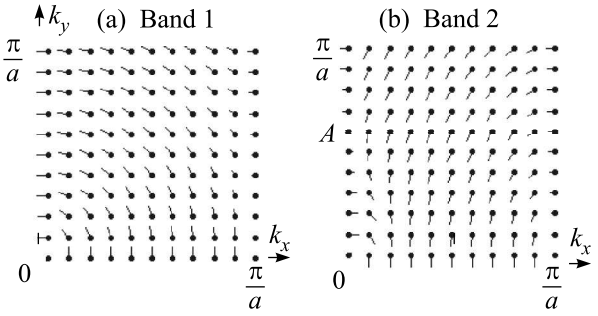

Fig.3. Spin polarization shown in one quarter of the BZ for the lowest band 1 (a) and the next band 2 (b). In the latter case the anticrossing takes place at point A, leading to the spin flip in the (k_x, k_y) plane. The parameters are the same as in Fig.2

for two lowest bands 1 and 2 shown in Fig.2. One can see that the spin polarization is qualitatively modified by periodic potential. The uniform curl distribution of spins which is typical for the 2DEG with SO interaction and without the periodic potential is conserved only near the BZ center. It can be seen in Fig.3a that the curl distribution is destroyed at the borders $k_x = \pm\pi/a$ of the BZ. The principal difference is that at $k_x = \pm\pi/a$ the spins are polarized along x axis and $\sigma_y = 0$, and a new type of singularity appears at $k_x = \pm\pi/a$, $k_y = 0$. More complicated picture shown in Fig.3b takes place for the spin polarization in the next energy band 2 shown in Fig.2. We see that at the BZ center the curl topology of spin polarization (with reversed angular velocity since $\lambda = 1$ for the upper Rashba band) is again unchanged. The

greatest changes from the uniform curl distribution also happen near the borders $k_x = \pm\pi/a$ of the BZ where a new curl has emerged. Another important feature of this spin distribution is the spin flip at the point A for band 2 shown on the axis $k_x = 0$ in the BZ. One can easily establish this point as the anticrossing point for the energy spectrum $\varepsilon = \varepsilon(k_x = 0, k_y)$ shown in Fig.2b. It should be mentioned that such effect was studied previously in quantum wires with SO interaction [4]. Besides, one can mention in Fig.3 that at certain points in the BZ the spin average values are decreased. The nature of such behavior is the mutual influence of SO terms and periodic potential and will be discussed below.

Another effect which can be promising for the application of SO superlattices can be found when an external electric field in the y direction is applied. Under these conditions the spin distribution in the BZ is shifted homogeneous along k_x which can produce the magnetization along x direction. It is clear that the sign of this magnetization changes with the direction of the E_y component of the external electric field and thus can be easily controlled.

3. Spinor symmetry and selection rules. *3.1. Spin parity.* The symmetry of the confinement potential $V(x) = V(-x)$ leads to the existence of an additional quantum number called the spin parity [5]. Namely, the Hamiltonian (1) commutes with the spin parity operator

$$\hat{S}_x = \hat{P}_x \hat{\sigma}_x, \tag{14}$$

where $\hat{P}_x$ is the inversion operator of the x coordinate, $\hat{P}_x f(x) = f(-x)$. We shall study the x-dependence of the spinor components $\psi^{1,2}(x)$ of quantum state (6). Below we demonstrate that the Bloch spinors in our problem taken at the points $\mathbf{k} = (k_x = 0, \pm\pi/a, k_y)$ can be labeled by a certain quantum number s which is the spin parity. In this case the spinor components $\psi^{1,2}(x)$ of (6) satisfy the following symmetry relations:

$$\psi^{1,2}_{\mathbf{k}}(x) = s\,\psi^{2,1}_{\mathbf{k}}(-x), \tag{15}$$

where $s = \pm 1$ is the spin parity.

In Fig.4b,c we show the x-dependence of the spinor components $\psi^{1,2}(x)$ in a superlattice elementary cell together with the superlattice potential $V(x)$ shown in Fig.4a. One can see that the spinor components $\psi^{1,2}(x)$ are real at $k_x = \pm\pi/a$. The states are taken at opposite k_y momentum components and for two neighboring energy bands 1 and 2. By comparing Fig.4a and 4b, 4c one can see that the space symmetry of a particular wavefunction on the superlattice period does not follow the symmetry of the superlattice potential $V(x)$.

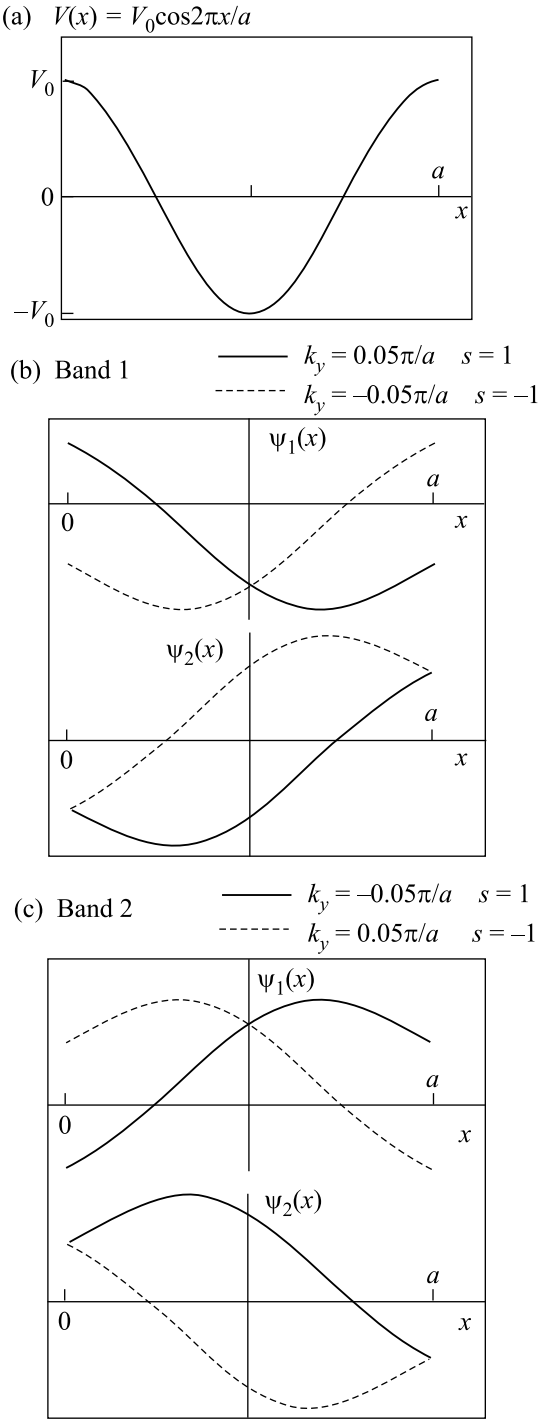

Fig.4. (a) Suprelattice potential $V(x)$ and (b), (c) space dependence of the spinor components $\psi^{1,2}(x)$ in a superlattice elementary cell at $k_z = \pi, a$, $k_y = 0.05 \pm \pi/a$ shown (b) for the lowest band 1 and (c) for the next band 2. The spin parity s changes from band 1 to band 2 and when $k_y \to -k_y$

The reason is the SO coupling which produces the space shift of the components $\psi^{1,2}(x)$ of the spinor (6). Such

effect was observed previously for the case of quasi one-dimensional SO systems [2]. Another important feature which can be seen in Fig.4 is that the spin parity changes both from the lowest band 1 to the higher band 2 and it changes also under the reflection $k_y \to -k_y$. In the next Section we shall see how these properties influence on the optical selection rules for the interband transitions.

The symmetry relation (15) leads to the following property of the spin density distribution (12):

$$S_{y,z}(x) = -S_{y,z}(-x). \qquad (16)$$

Since the spinor components $\psi^{1,2}(x)$ are real at $k_x = \pm\pi/a$, the S_y component of spin density vanish identically. So, we calculate the space distribution of the other components, $S_x(x)$ and $S_z(x)$ taken for the point $k_x = \pi/a$, $k_y = \pm 0.05\pi/a$ in the BZ of the lowest energy band (the corresponding spin polarization which is the space integral of $S_{x,y}$ is shown above in Fig.3a). It should be stressed that in SO superlattice the S_z component transverse to the superlattice plane appears while it is absent in pure Rashba 2DEG. The results for $S_x(x)$, $S_z(x)$, and the x-dependence of the two-dimensional vector $(S_x(x), S_z(x))$ are shown in Fig.5. One can see that the average values of the spin density across the superlattice cell shown in Fig.5 are close to zero which can be seen also in Fig.3 in the vicinity of the point $k_x = \pi/a$, $k_y = \pm 0.05\pi/a$ where no clear indication of an arrow is seen. In Fig.5 it is clear also that the spin components change their signs when the k_y momentum projection is changed, thanks to the change of the spin parity quantum number observed above. In more details this effect can be explained with the help of the operator composition for the reflection in the reciprocal space. Namely, the transformation $\hat{K}_y = k_y \to -k_y$ at the BZ boundary $k_x = \pm\pi/a$ is equivalent to the inversion operator $\hat{K} = \mathbf{k} \to -\mathbf{k}$ since the lines $k_x = \pm\pi/a$ are topologically identical and one can write $\hat{K}_y\hat{K}_x = \hat{K}$ where $\hat{K}_x = k_x \to -k_x$ and $\hat{K}_x = \hat{1}$ at the BZ border $k_x = \pm\pi/a$. Thus, the reflection of k_y here produces the same effect as the inversion $\mathbf{k} \to -\mathbf{k}$, the latter giving us the spin flip. As it was mentioned earlier, the spin parity and the corresponding symmetry relation for it at $k_y \to -k_y$ should exist also at $k_x = 0$. Indeed, at $k_x = 0$ the operation $k_y \to -k_y$ is also identical to $\mathbf{k} \to -\mathbf{k}$ thus producing the change $s \to -s$ and making a spin flip.

By looking onto Fig.5b,c, one can call the spin density distribution inside the superlattice elementary cell as a standing spin wave. From Fig.5b,c one can see that the wriggling takes place with the opposite direction for the opposite k_y components of the electron momenta in accordance with the symmetry properties discussed above.

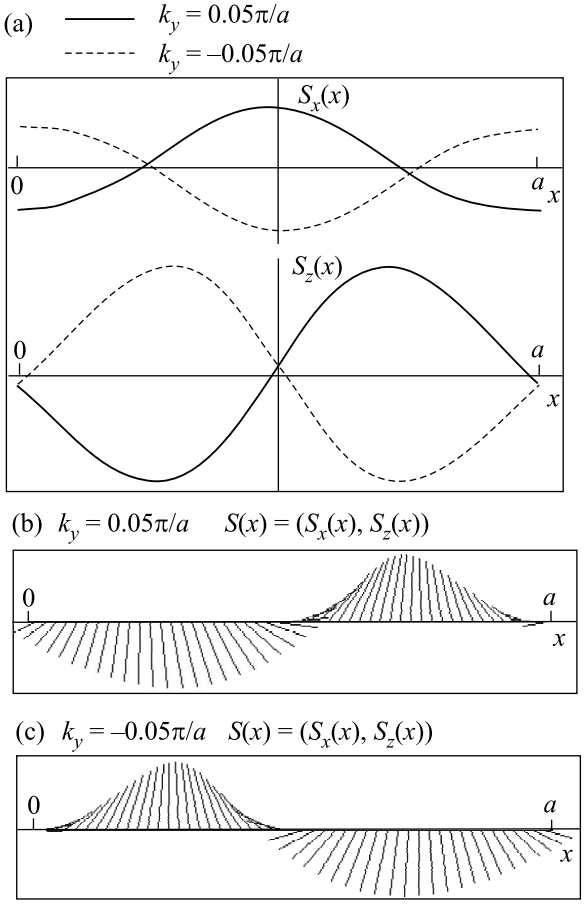

Fig.5. (a) spin density distribution $S_x(x)$, $S_z(x)$ and (b), (c) the x-dependence of the 2D spin vector $(S_x(x), S_z(x))$ shown for the lowest band 1 (see Fig.2) at $k_x = \pi/a$, $k_y = \pm 0.05\pi/a$. The spin components switch their signs when the k_y momentum projection is reflected due to the change of the spin parity quantum number. Inside the superlattice elementary cell one can observe in (b) and (c) the spin standing wave with the spin wriggling in opposite directions for the opposite k_y components of the electron momentum

3.2. Selection rules. The analysis of the optical properties of the SO superlattices requires the knowledge of corresponding selection rules. We discuss here the selection rules for the operator of the dipole momentum $\hat{x}$. The symmetry analysis of the wavefunction carried out above will help us to define the selection rules for the certain points in the BZ $k_x = 0, \pm\pi/a$ which are often correspond to the energy minima and maxima. By considering the symmetry properties (15) of the spinor (6) one can see that the matrix element

$$M^{ss'}_{mm'k} = \langle \psi_{msk} \mid \hat{x} \mid \psi_{m's'k} \rangle \qquad (17)$$

for the direct transitions between the bands m and m' having the spin parity s and s' is equal to

$$M^{ss'}_{mm'k} = (1 - ss')M_{mm'k}. \qquad (18)$$

Here $M_{mm'k}$ is an integral independent of spin parity and in general it is non-zero. So, the direct optical transitions are allowed only between the states of the opposite spin parity. For example, for our problem the states in two lowest neighboring spin-split bands 1 and 2 discussed above satisfy to this condition and the direct transitions between them are thus possible.

In conclusion we would like to mention also that in the presence of and external constant electric field parallel to the superlattice direction one can expect a simultaneous appearance of wriggling electron trajectories (*zitterbewegung* [14]) and Bloch oscillations. Such situation may lead to non-trivial dynamics and transport of charged particles, and we plan to investigate these problems in a separate paper.

This work was supported by the Program "Development of the Higher school research potential" (2006), by the Russian Foundation for Basic Research grant # 05-02-16449, by the CRDF Award # RUX0-001-NN-06, and by the Dynasty Foundation.

1. E. I. Rashba, Fiz. Tverd. Tela (Leningrad) **2**, 1224 (1960) [Sov. Phys. Solid State **2**, 1109 (1960)]; Y. A. Bychkov and E. I. Rashba, Pis'ma Zh. Éksp. Theor. Fiz. **39**, 66 (1984) [JETP Lett. **39**, 78 (1984)].
2. A. V. Moroz and C. H. W. Barnes, Phys. Rev. B **60**, 14272 (1999).
3. F. Mireles and G. Kirczenow, Phys. Rev. B **64**, 024426 (2001); X. F. Wang and P. Vasilopoulos, Phys. Rev. B **67**, 085313 (2003).
4. M. Governale and U. Zülicke, Phys. Rev. B **66**, 073311 (2002).
5. S. Debald and B. Kramer, Phys. Rev. B **71**, 115322 (2005).
6. X. F. Wang, Phys. Rev. B **69**, 035302 (2004).
7. I. Vurgaftman and J. R. Meyer, Phys. Rev. B **70**, 205319 (2004).
8. P. Kleinert, V. V. Bryksin, and O. Bleibaum, Phys. Rev. B **72**, 195311 (2005).
9. G. Engels, J. Lange, Th. Schapers et al., Phys. Rev. B **55**, 1958R (1997); B. Das, D. C. Miller, S. Datta et al., Phys. Rev. B **39**, 1411 (1989); J. Luo, H. Munekata, F. F. Fang et al., Phys. Rev. B **41**, 7685 (1990).
10. S. D. Ganichev, V. V. Bel'kov, L. E. Golub, et al., Phys. Rev. Lett. **92**, 256601 (2004).
11. S. Murakami, N. Nagaosa, and S. C. Zhang, Science **301**, 1348 (2003); J. Wunderlich, B. Kaestner, J. Sinova et al., Phys. Rev. Lett. **94**, 047204 (2005).
12. S. D. Ganichev, V. V. Bel'kov, P. Schneider et al., Phys. Rev. B **68**, 035319 (2003).
13. J. B. Miller, D. M. Zumbühl, C. M. Marcus et al., Phys. Rev. Lett. **90**, 076807 (2003).
14. J. Schliemann, D. Loss, and R. M. Westervelt, Phys. Rev. Lett. **94**, 206801 (2005).